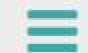

EN

Dergi Listesi

Dergi Adı

ISSN 0925-3467

Yıl 2021

Temizle Ara

No	Yıl	Dergi Adı	ISSN	Çeyreklik Grup	Katsayı	kategori	Dergi Puanı
100710	2021	OPTICAL MATERIALS	0925-3467	Q2	0.8	SCIE	

Sayfada 10 Kayıt Göster

1 Kayıttan 1 - 1 Arası Kayıtlar

Optical Materials 129 (2022) 112480

Contents lists available at ScienceDirect

Optical Materials

journal homepage: www.elsevier.com/locate/optmat

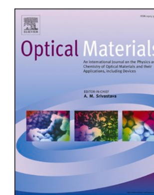

Optical and nano-mechanical characterization of *c-axis* oriented AlN film

Padmalochan Panda [a], Ramaseshan Rajagopalan [a,*], S. Tripursundari [b], Ismail Altuntas [b], Ilkay Demir [b]

[a] Surface and Nanoscience Division, Materials Science Group, Indira Gandhi Centre for Atomic Research, A CI of Homi Bhabha National Institute, Kalpakkam, 603102, India

[b] Nanophotonics Application and Research Center, Department of Nanotechnology Engineering, Sivas Cumhuriyet University, 58140, Sivas, Turkey

ARTICLE INFO

Keywords:
c-axis AlN thin Film
Elipsometry
Uniaxial anisotropic
Thermo-optic coefficients
Refractive index
Nano-mechanical
Surface energy

ABSTRACT

This paper reports the temperature effects on the optical properties of metalorganic vapour-phase epitaxy (MOCVD) grown c-axis oriented AlN epilayer thin film studied by in-situ high-temperature spectroscopic ellipsometry. The crystal structure and the quality of the grown AlN epilayer film are analyzed using X-ray Diffraction and rocking curve techniques, respectively. Modelling of the ellipsometric data revealed that the uniaxial anisotropic refractive indices of the *c-axis* oriented film in the directions $n_{\|}$ and $n_{\perp}$ increased from 2.50 to 2.59 and 2.32 to 2.37, respectively with the increase in temperature from 223 to 573 K. The thermo-optic coefficients were evaluated to be around 10^{-5}. Nano-mechanical characterization of this film showed an average hardness of 19.4 GPa at ambient temperature, which is higher than *a-axis* oriented AlN film. The average surface free energy of the synthesized film as evaluated from contact angle measurements is reported to be around 36.22 ± 0.64 mN/m. These results are highly relevant for a better understanding of *c-axis* oriented AlN-based materials in high-temperature ultraviolet optical devices.

1. Introduction

Thin films of AlN have received widespread scrutiny in the semiconductor industry due to its unique mechanical and optical properties [1–8]. Also, doping from transition elements, the mechanical properties and semiconductor of AlN can be improved multifold [9–12]. The hexagonal crystal-field and spin orbital splittings generate two configurations of the excitonic transitions *i.e.* π ($E\|c$, c = axis of wurzite structure) and $\sigma(E\perp c)$, in the top of the valence band of the wurtizite AlN.s [13,14]. This results in a strong optical uniaxial anisotropic behavior for *c-axis* AlN.The reports on optical properties of c-axis AlN oriented and epitaxial thin films at ambient and high temperatures are few. But they are not perfect epitaxy with full width at half maximum (FWHM) lower than 0.42 in x-ray rocking curve studies. For the use of AlN in deep ultraviolet light-emitting diode (UV-LED) application, knowledge of the refractive indices of the material with temperature and plane of orientation of the material is essential. Because, the extracted light intensity of the LEDs is directly determined by the critical angle of light escape cone which inversely depends on a function of refractive index [15]. Additionally, AlN is used as distributed bragg reflectors (DBR) for group-III Nitride based laser owing a very high refractive index in UV–visible rang [16]. In general, the operating temperature of the laser increases the refractive index of AlN based DBR that affects both the resonance wavelength and the gain spectrum of laser. Therefore, the temperature-dependent refractive index, known as the thermo-optic effect of an oriented material should be investigated for better performance of various devices [17,19].

Nevertheless, the temperature-dependent optical study on *c-axis* oriented AlN film has been limited only to the isotropic response as discussed in the previous literature [19–22]. Therefore, it is crucial and relevant to investigate the nature of the anisotropic optical constant of high-quality *c-axis* oriented AlN thin film with temperature. Since *c-axis* AlN film is mainly used in optoelectronic devices, it is also important to investigate the nanomechanical properties since the contact loading/unloading during fabrication deteriorates the performance of the devices. In this report, we have basically explored the uniaxial anisotropic behavior of *c-axis* AlN thin film at different temperatures. Other surface characteristics such as the depth dependant indentation hardness and the surface free energies of the film were also determined using nanoindentation and contact angle measurements, respectively.

* Corresponding author.
E-mail addresses: seshan@igcar.gov.in (R. Rajagopalan), sundari@igcar.gov.in (S. Tripursundari).

https://doi.org/10.1016/j.optmat.2022.112480
Received 8 March 2022; Received in revised form 28 April 2022; Accepted 9 May 2022
Available online 19 May 2022
0925-3467/© 2022 Elsevier B.V. All rights reserved.

2. Experimental details

2.1. Film growth & structure determination

AlN film with *c-axis* orientation were grown using an Aixtron 200/4 RF-S low pressure, horizontal flow metalorganic vapour-phase epitaxy (MOCVD) system on sapphire substrates. The growth was started first at low temperature with ≈45 nm AlN nucleation layer. Then AlN layer was grown using PALE (Pulsed Atomic Layer Epitaxy) technique at high temperature, a detailed synthesis process are discussed elsewhere [23]. The crystal structure of this film was studied by parallel beam geometry (Cu - K_α) X-ray Diffraction (XRD) geometry.

2.2. Ellipsometry measurements and modeling

The optical constants such as refractive index (n) and extinction coefficient (k) of thin films are determined accurately using spectroscopic ellipsometry (SE), from the changes in polarization of linearly polarized incident light in terms of amplitude (Ψ) and phase (Δ), upon reflection from the films. The complex reflectance ratio (ρ) *i.e* ratio of complex reflection coefficients namely r_p and r_s are measured from SE and is given by

$$\rho = \frac{r_p}{r_s} = e^{i\Delta} tan\Psi \tag{1}$$

where p and s are the parallel and perpendicular components of the reflected light with respect to the plane of incidence [24]. In this study, a phase modulated ellipsometer (M/s. Horiba Jobin-Yvon, UVISEL2, France) is used to compute the optical constants. The phase modulated SE experimentally measures I_s and I_c which are related to the ellipsometric parameters Ψ and Δ in the following way [25],

$$I_s = sin(2\Psi)sin(\Delta) \quad and \quad I_c = sin(2\Psi)cos(\Delta) \tag{2}$$

The I_s and I_c are measured at light incident angles of 65, 70 and 75° with the normal to the *c-axis* AlN film surface in an energy range of 1.5–6 eV. The n and k of the *c-axis* AlN film are extracted by fitting the measured experimental parameter I_s and I_c. A modified Forouhi-Bloomer dispersion relation that fits steadily for wide wavelength range covering from normal to anomalous dispersion region is executed to extract the n and k with one oscillator term. This dispersion relation is also compatible with Kramers-Kronig relation with five independent parameters as narrated below.

$$n(\omega) = n_\infty + \sum_{j=1}^{N} \frac{B_j(\omega - \omega_j) + C_j}{(\omega - \omega_j)^2 + \Gamma_j^2} \tag{3}$$

$$k(\omega) = \begin{cases} \sum_{j=1}^{N} \frac{f_j(\omega - \omega_g)^2}{(\omega - \omega_j)^2 + \Gamma_j^2} & : \omega > \omega_g \\ 0 & : \omega \le \omega_g \end{cases} \tag{4}$$

here, the strength of oscillator is denoted as f_j (in eV), the absorption peak broadening is denoted as Γ_j (in eV), the energy at the maximum value of extinction coefficient is denoted as ω_j (in eV), and the energy at the minimum value of absorption is denoted as ω_g (in eV) [26].

A DeltaPsi2 software from Horiba Jobin-Yvon is used to carry out the data analysis and anisotropic fitting by suitable models based on the approaches mentioned in the literature [18,27–31]. A systematic estimate of the inclusion and omission of layers have been pursued for the analysis of optical constants of *c-axis* AlN film in which, a five layer model consisting of Air/roughness (AlN + void)/AlN/nucleation layer of AlN/Al_2O_3 with uniaxial anisotropic conditions has been employed. The Bruggeman Effective Medium Approximation is used to evaluate the roughness of the film. The goodness of fitting is expressed in terms of χ^2 value using classical non-linear minimization Levenberg-Marquardt algorithm as shown in below equation.

$$\chi^2 = \frac{1}{2N - P - 1} \sum_{i=1}^{N} \left[\left(\frac{I_{s,m_i} - I_{s,c_i}}{10^{-2}} \right)^2 + \left(\frac{I_{c,m_i} - I_{c,c_i}}{10^{-2}} \right)^2 \right] \tag{5}$$

here N denotes the total number of data points, P denotes to the total number of fitted parameters and indices m_i and c_i are to the measured & computed ellipsometry parameters for the i_{th} energy [25]. For all SE data fitting, the χ^2 value lies between 10 and 20 in the incident light energy ranging from 1.5 to 6 eV. For the temperature-dependant ellipsometric measurements, the film are placed in a LINKAM THMSEL 350 temperature-controlled elipsometer stage. The chamber of this stage is maintained at a vacuum of $\sim 10^{-3}$ mbar using an oil-free diaphragm pump to avoid condensation and contamination. Ellipsometric parameters were measured in the temperature range 223–573 K in steps of 50 K. It is to be added that the temperature of the specimen through out the measurement is maintained at $\sim \pm 0.1$ °C. The ellipsometric parameters are computed after eliminating the contribution from windows of the LINKAM stage using a standard Si single crystal [17].

2.3. Nanomechanical characterization

The nanomechanical properties of *c-axis* AlN thin film were carried out by a compact platform Ultra Nano-indentation Tester (M/s. Anton Paar, Switzerland) furnished by a Berkovich diamond tip with end radius of 30 nm. Indentation was performed as a function of depth (15–450 nm) at different linear load with the standard process *i.e.* the loading and unloading rates are maintained as twice of the peak load (continuous stifness mode). The indentation hardness and modulus of the synthesized film were analyzed from the load and displacement curve using the principle of Oliver and Pharr model [32].

2.4. Surface free energy measurement

Surface free energy of AlN thin film was calculated from contact angle (CA) measurements performed using two liquids, viz water and diiodo-methane in sessile drop geometry using contact angle goniometer (KRUSS DSA100 Drop Shape Analyzer system).

3. Results and discussion

3.1. Structural study by XRD

XRD profile of AlN thin film grown on sapphire (Al_2O_3) substrate is shown in Fig. 2. It exhibits a strong (002) peak corresponding to wurtzite hexagonal structure of AlN at 36.10°, with FWHM 0.02° and concur with the ICDD data 25-1133. This signifies that this is a highly oriented epilayer AlN film along *c-axis* direction. AlN with both wurtzite and zinc blende structures have polar axes (lack of inversion symmetry) along the bonds in the ⟨0001⟩ direction and ⟨111⟩ direction for wurtzite and zinc blende, respectively and are all faced by nitrogen in the same direction

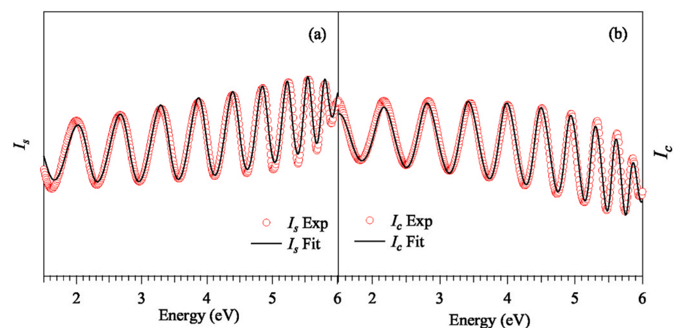

Fig. 1. The measured parameters as I_s and I_c and their corresponding fit of *c-axis* AlN film at 323 K.

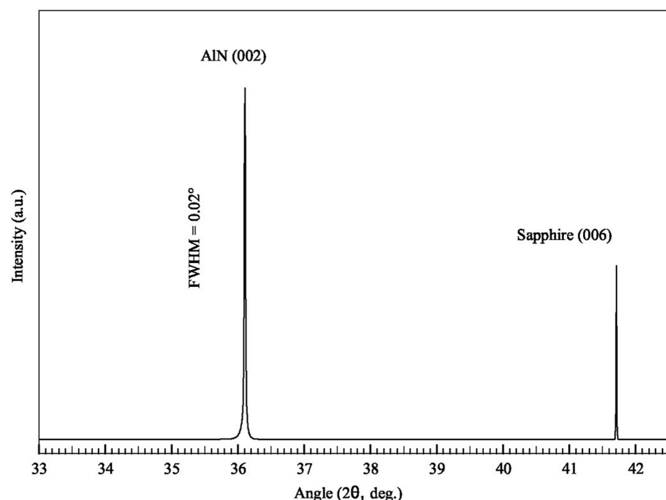

Fig. 2. XRD profiles of *c-axis* AlN thin film on sapphire substrate.

of the cation [33]. For further confirmation about the orientation of plane, mosaicity (misorientation of crystallites) and dislocations in the plane, rocking curve technique is used for (002) plane and is shown in Fig. 3. The result reveals that this film is highly oriented along *c-axis* direction with FWHM of 0.0142 ± 0.0003 at the angle 18.05° (FWHM = 51.12 arcsec), which is lower than the reported values [34–36]. The threading dislocation density along the*c-axis* direction of this AlN film is calculated using the following equation [37].

$$\rho_{TD} = \frac{\Gamma}{6.283 ln2b^2} \tag{6}$$

where ρ_{TD} is the threading dislocation density, Γ is the FWHM of the rocking curve for (002) plane after excluding the contribution from the instrumental broadening, b is the Burger vector of AlN ($b = 0.497$ nm). In this study, the threading dislocation density is obtained as 4.78×10^6 cm^{-2}, which is also lower than the reported values by Uesugi et al. and Chenguang et al. as 2.07×10^8 cm^{-2} and 4.7×10^7 cm^{-2}, respectively [38,39].

In the present experiment AlN film oriented in c-axis and possess wurzite crystal structure that exhibits anisotropy optical properties. Therefore, it is imperative to study its anisotropic optical response in both parallel and perpendicular directions to the surface normal.

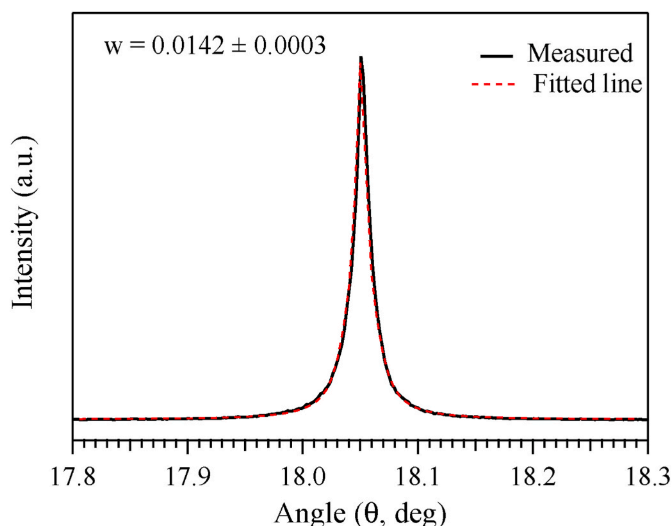

Fig. 3. Rocking curve of *c-axis* orientation of AlN thin film on sapphire substrate.

3.2. Behavior of optical constants with temperatures

The measured experimental (red circle) and corresponding fitting (black lines) of ellipsometric parameters (I_s and I_c) for *c-axis* AlN film at 323 K is shown in Fig. 1 as a representative for all other temperatures. It can be seen that the parameters I_s and I_c across the whole spectral range of 1.5–6 eV are well fitted. From SE modeling, the thickness of the film layers as computed as are 10, 480 and 46 nm for roughness, AlN and nucleation layer of AlN, respectively.

Also, to know the temperature dependent optical constants of *c-axis* AlN film, the SE measurement are performed in the temperature range of 223–573 K. The anisotropic complex refractive index of *c-axis* AlN film at various temperature acquired from the five layer model are manifested in Fig. 4 and Fig. 5, respectively. It is observed that both the n and k reveal a strong uniaxial anisotropic behavior and increase monotonically with increasing the incident light energy. Since, AlN is an ideal candidate for deep-UV LED or optoelectronic devices, it will therefore be certainly worthwhile to investigate the effect of temperature on both n and k of the *c-axis* AlN film at 210 nm (5.9 eV) and is plotted the same in Fig. 6.

With the increase in temperature from 223 to 573 K, both n ($n_{\parallel}$ and $n_{\perp}$) and k ($k_{\parallel}$ and $k_{\perp}$) increases marginally. The values of $n_{\parallel}$ and $n_{\perp}$ increased from 2.50 to 2.59 and from 2.32 to 2.37, respectively, while the values of $k_{\parallel}$ and $k_{\perp}$ also increased from 0.048 to 0.082 and from 0.0015 to 0.0042, respectively with the increase in temperature from 223 to 573 K. With increase in temperature, electrons gets sufficient energy to excite higher state and inter-band transition becomes dominant near to band edge. So the k value increase rapidly with temperature and shows a semiconductor nature. This result is also very similar to Liu et al. [22], where he has reported as isotropic behavior of *c-axis* AlN. The literature results are summarized in Table 1 by comparing the anisotropic refractive index of *c-axis* AlN with this work at 210 nm (room temperature).

Fig. 7 shows a representative thermo-refractive coefficients dn/dT and dk/dT as a function of incident energy computed on the basis of a procedure outlined by Winsemius et al., assuming that n and k vary linearly with temperature [40]. This thermo-refractive coefficients ($dn_{\parallel}/dT$ and $dn_{\perp}/dT$) are comparable with Watanabe et al. [19]. However, the imaginary part of the thermo-refractive coefficients have not been reported by any of the authors for AlN films.

3.3. Nanomechanical properties

Nano-indentation technique is employed to study the Nano-mechanical properties of *c-axis* oriented AlN film as a function of depth (15–450 nm) to understand the deformation behavior. Fig. 8 and Fig. 9 show the indentation hardness (*H*) and modulus (*E*) of Al_2O_3 substrate and *c-axis* oriented AlN thin film as a function of depth. The indentation hardness (*H*) and indentation modulus (*E*) of the Al_2O_3 substrate are around 29 and 470 GPa, respectively. However, the *c-axis* AlN film on Al_2O_3 substrate shows a constant hardness value around 19.4 GPa from 15 to 250 nm and afterwards it increases slightly with depth. According to indentation thumb rule, the indentation on a thin film should be performed a depth lower than 1/10th of the total thickness the film to ascertain the film only hardness, by suitably avoiding the substrate effect [41–43]. In this study, the thickness of this AlN film is calculated as around 480 ± 56 nm by SE technique. Since the substrate is harder than this film, the hardness of the film increases gradually at higher depths due to the substrate effect, which is pronounced beyond 320 nm. The standard deviation of hardness is very small denotes that this film is quite uniform and homogeneous. Similarly, Modulus (*E*) of these film also increased moderately from 370 to 415 GPa with depth and reached near to the substrate modulus at higher depths, which is shown in Fig. 9.

Hardness of thin film generally depends on it's micro-structure, orientation, crystallite size and induced stress during the growth. In this study, AlN film is oriented along *c-axis* direction, that means all the

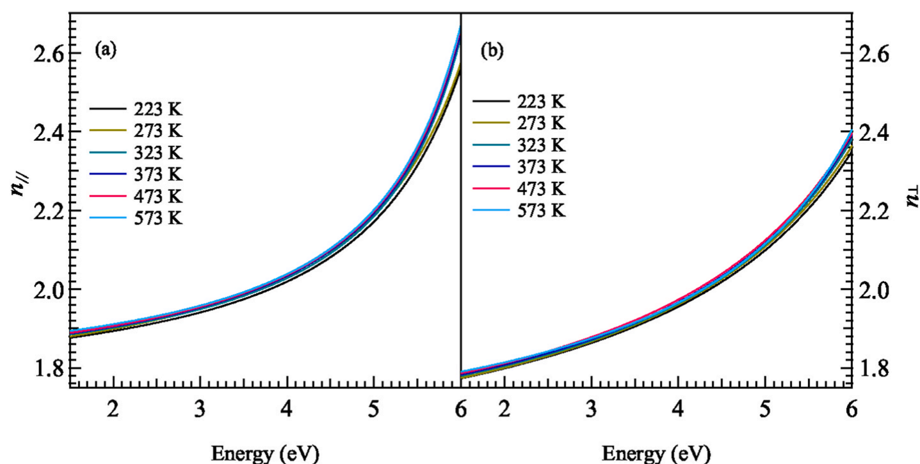

Fig. 4. Plot on refractive index (a) $n_{\|}$ and (b) $n_{\perp}$ against to energy at different film temperatures.

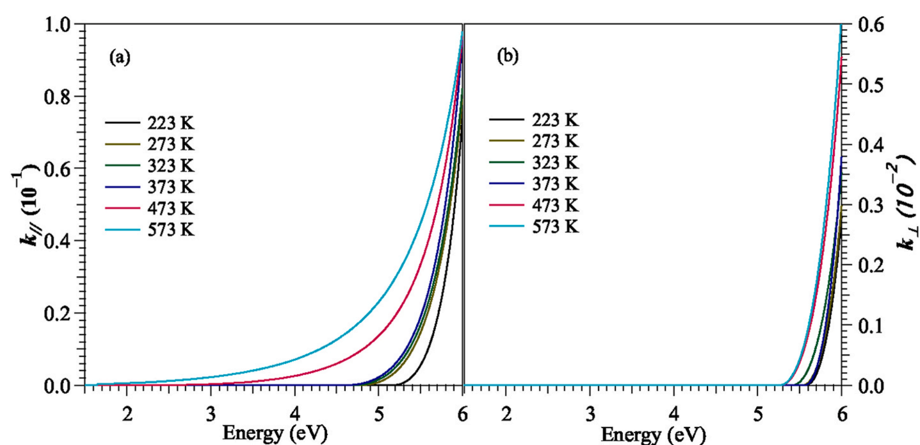

Fig. 5. Plot on extinction coefficients (a) $k_{\|}$ and (b) $k_{\perp}$ Vs energy at different film temperatures.

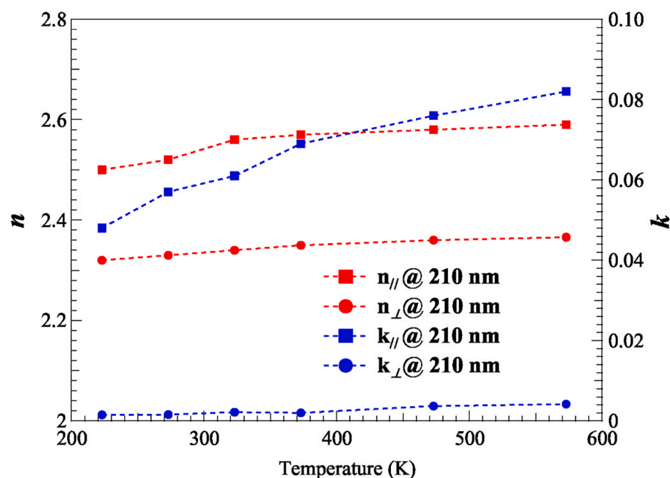

Fig. 6. Plot of *n* and *k* values at different film temperatures, for 210 nm energy.

c-planes are grown parallel to the substrate. For wurtzite hexagonal structure, the planner density is higher along *c-plane* compared to other planes. Hence, the *c-axis* plane oriented AlN is expected to show a higher hardness than other orientations. The indentation hardness measured for *c-axis* AlN was around 19.4 GPa, which is higher than *a-axis* AlN 17 GPa reported elsewhere [2].

Table 1
Anisotropic refractive index of *c-axis* AlN films at wavelength of 210 nm (room temperature).

$n_{\|}$	$n_{\perp}$	Ref.
~ 2.75	~ 2.74	[18]
	~ 2.55	[19]
~ 2.52	~ 2.33	this work

3.4. Contact angle of water and diiodo-methane

The CA for water and diiodomethane showed that the surface of AlN was hydrophilic. A typical measurement of H_2O on AlN is shown in Fig. 10. The surface free energy is computed from contact angles of H_2O and diiodo-methane using ORWK model was 36.22 ± 0.64 mN/m with the disperse and polar components 33.82 ± 0.39 and 2.4 ± 0.25 mN/m, respectively.

4. Conclusion

This paper reports temperature effects on refractive index of MOCVD grown c-axis oriented AlN epilayer thin film studied by in-situ high temperature spectroscopic ellipsometry. A modeling of the ellipsometric data revealed uniaxial anisotropic refractive indices of the c-axis oriented film directions $n_{\|}$ and $n_{\perp}$ increased from 2.50 to 2.59 and 2.32 to 2.37, respectively with the increase in temperature from 223 to 573 K. The thermo-optic coefficients were evaluated to be around 10^{-5}. Nano-

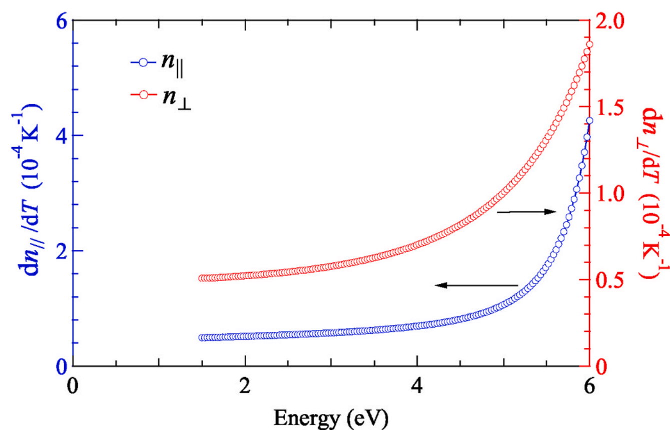

Fig. 7. Thermo-optic coefficients (($dn_{||}/dT$ and $dn_{\perp}/dT$) of *c-axis* AlN thin film for T_{avg} from 248 K to 523 K.

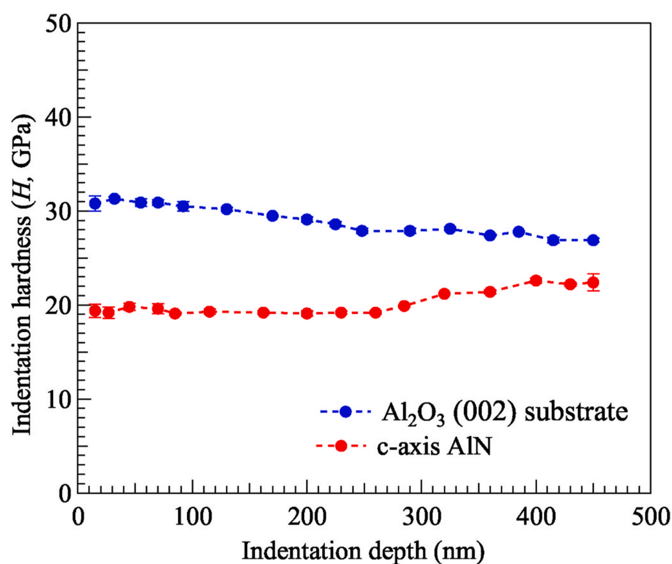

Fig. 8. Indentation hardness as a function of depth on Sapphire substrate and *c-axis* AlN film.

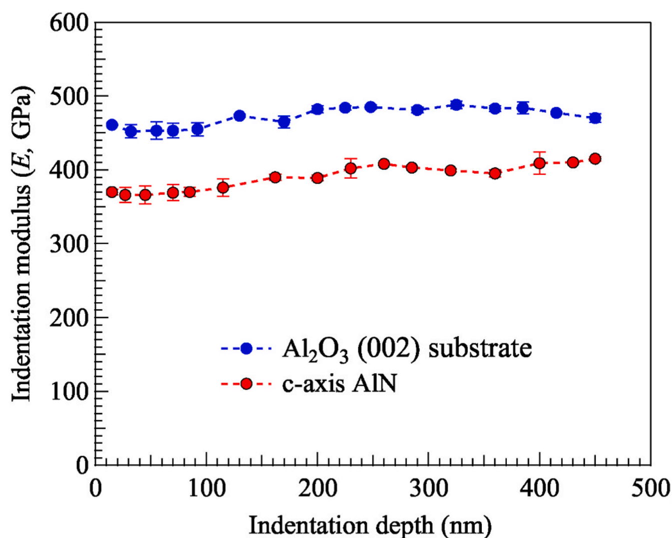

Fig. 9. Indentation modulus as a function of depth on Sapphire substrate and *c-axis* AlN film.

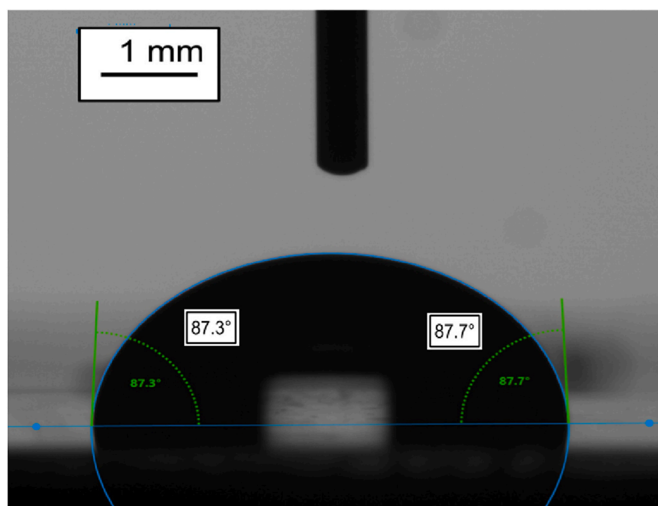

Fig. 10. A typical contact angle measurement using H_2O on AlN.

mechanical characterization of the film showed an average hardness of 19.4 GPa at ambient temperature, which is higher than a-axis oriented film. The average surface free energy of the grown film is reported to be around 36.22 ± 0.64 mN/m.

CRediT authorship contribution statement

Padmalochan Panda: Investigation, Formal analysis, Writing – original draft. **Ramaseshan Rajagopalan:** Conceptualization, Writing – review & editing, Supervision. **S. Tripursundari:** Methodology, Validation, Writing – review & editing. **Ismail Altuntas:** Investigation, Validation. **Ilkay Demir:** Investigation, Validation.

Declaration of competing interest

The authors declare that they have no known competing financial interests or personal relationships that could have appeared to influence the work reported in this paper.

Acknowledgment

We acknowledge Mr.Venkateswara Reddy Karrevula, SRF who has recorded the contact angle measurement. This work is partially supported by the TUBITAK under Project Number 118F425.

References

[1] H. Morkoc, Handbook of Nitride Semiconductors and Devices 1, WILEY-VCH, Weinheim), 2008. Materials Properties, Physics and Growth.
[2] F. Jose, R. Ramaseshan, S. Tripura Sundari, S. Dash, A.K. Tyagi, M.S.R.N. Kiran, U. Ramamurty, Appl. Phys. Lett. 101 (2012), 254102.
[3] X.H. Ji, S.P. Lau, G.Q. Yu, W.H. Zhong, B.K. Tay, J. Phys. Appl. Phys. 37 (2004) 1472–1477.
[4] P. Panda, R. Ramaseshan, N. Ravi, G. Mangamma, F. Jose, S. Dash, K. Suzuki, H. Suematsu, Mater. Chem. Phys. 200 (2017) 78–84.
[5] V. Chivukula, D. Ciplys, A. Sereika, M. Shur, J. Yang, R. Gaska, Appl. Phys. Lett. 96 (2010), 163504.
[6] T. Aoki, N. Fukuhara, T. Osada, H. Sazawa, M. Hata, T. Inoue, APEX 7 (2014), 106502.
[7] E. Yarar, V. Hrkac, C. Zamponi, A. Piorra, L. Kienle, E. Quandt, AIP Adv. 6 (2016) 75115.
[8] G. Chen, Y. Zhang, H. Zhang, L. Xie, Z. Xing, Z. Cheng, H. Li, Y. Xiao, H. Liang, H. Liu, X. Xie, L. Bia, G. Liu, Opt. Mater. 111 (2021), 110678.
[9] F. Jose, R. Ramaseshan, S. Dash, S. TripuraSundari, D. Jain, V. Ganesan, P. Chandramohan, M. Srinivasan, A. Tyagi, B. Raj, Mater. Chem. Phys. 130 (2011) 1033–1037.
[10] P. Panda, R. Ramaseshan, M. Sahoo, N.G. Krishna, A.K. Yadav, S.N. Jha, D. Bhattacharyya, Phys. Chem. Chem. Phys. 20 (2018), 13084.
[11] X.Y. Cui, D. Fernandez-Hevia, B. Delley, A.J. Freeman, C. Stampfl, J. Appl. Phys. 101 (2007), 103917.

[12] M.C. Portillo, S.G. Hernández, Y.P. Bernal, M. Velis, J.V. Cab, S. Alcántara, J. Alvarado, Opt. Mater. 108 (2020), 110206.
[13] L. Chen, B.J. Skromme, R.F. Dalmau, R. Schlesser, Z. Sitar, C. Chen, W. Sun, J. Yang, M.A. Khan, M.L. Nakarmi, J.Y. Lin, H.X. Jiang, Appl. Phys. Lett. 85 (2004) 4334–4336.
[14] E. Silveira, J.A. Freitas, O.J. Glembocki, G.A. Slack, L.J. Schowalter, Phys. Rev. B 71 (2005), 041201.
[15] E.F. Schubert, in: Light Emitting Diodes, second ed., Cambridge University Press, 2006.
[16] C.C. Chen, M.H. Shih, Y.C. Yang, H.C. Kuo, Appl. Phys. Lett. 96 (2010), 151115.
[17] S. Tripura Sundari, R. Ramaseshan, F. Jose, S. Dash, A.K. Tyagi, J. Appl. Phys. 115 (2014) 33516.
[18] W. Jiang, W. Lin, S. Li, J. Chen, J. Kang, Opt. Mater. 32 (2010) 891–895.
[19] N. Watanabe, T. Kimoto, J. Suda, J. Appl. Phys. 104 (2008), 106101.
[20] H. He, L. Huang, Y. Zhang, Y. Fu, X. Shen, J. Zeng, Vacuum 100 (2014) 33–35.
[21] M. Feneberg, M.F. Romero, B. Neuschl, K. Thonke, M. Röppischer, C. Cobet, N. Esser, M. Bickermann, R. Goldhahn, Thin Solid Films 571 (2014) 502–505.
[22] Y. Liu, E. Ghafari, X. Jiang, Y. Feng, Z.C. Feng, I. Ferguson, N. Lu, MRS Advances 2 (2017) 323–328.
[23] I. Demir, H. Li, Y. Robin, R. McClintock, S. Elagoz, M. Razeghi, J. Phys. Appl. Phys. 51 (2018) 85104.
[24] P. Panda, R. Ramaseshan, S.T. Sundari, Opt. Mater. 118 (2021), 111245.
[25] M. Modreanu, J. Sancho-Parramon, O. Durand, B. Servet, M. Stchakovsky, C. Eypert, C. Naudin, A. Knowles, F. Bridou, M.F. Ravet, Appl. Surf. Sci. 253 (2006) 328–334.
[26] P. Loper, M. Stuckelberger, B. Niesen, J. Werner, M. Filipic, S.J. Moon, J.H. Yum, M. Topic, S. De Wolf, C. Ballif, J. Phys. Chem. Lett. 6 (2015) 66–71.
[27] P. Panda, R. Ramaseshan, S.T. Sundari, H. Suematsu, OSA Continuum 1 (2018) 1241–1250.
[28] L.P. Wang, D.S. Shim, Q. Ma, V.R. Rao, E. Ginsburg, A. Talalyevsky, J. Vac. Sci. Technol. 23 (2005) 1284–1289.
[29] S. Shokhovets, R. Goldhahn, G. Gobsch, S. Piekh, R. Lantier, A. Rizzi, V. Lebedev, W. Richter, J. Appl. Phys. 94 (2003) 307–312.
[30] M.I. Kang, S.W. Kim, Y.G. Kim, J.W. Ryu, J. Kor. Phys. Soc. 57 (2010) 389–394.
[31] M. Gaillet, Yan, E. Teboul, Thin Solid Films 516 (2007) 170–174.
[32] W. Oliver, G. Pharr, J. Mater. Res. 19 (2004) 3–20.
[33] O. Ambacher, J. Majewski, C. Miskys, A. Link, M. Hermann, M. Eickhoff, M. Stutzmann, F. Bernardini, V. Fiorentini, V. Tilak, B. Schaff, L.F. Eastman, J. Phys. Condens. Matter 14 (2002) 3399–3434.
[34] F. Martin, P. Muralt, M.A. Dubois, A. Pezous, J. Vac. Sci. Technol. 22 (2004) 361.
[35] L. Iriarte, R. Chistyakov, Appl. Surf. Sci. 396 (2017) 129–137.
[36] W. Jianliang, G. Pharr, J. Mater. Res. 19 (2004) 3–20.
[37] C. Romanitan, I. Mihalache, O. Tutunaru, C. Pachiu, J. Alloys Compd. 858 (2021), 157723.
[38] K. Uesugi1, Y. Hayashi, K. Shojiki, H. Miyake, J. Mater. Res. 12 (2019) 65501.
[39] C. He, W. Zhao, H. Wu, S. Zhang, K. Zhang, L. He, N. Liu, Z. Chen, B. Shen, Cryst. Growth Des. 12 (2018) 6816–6823.
[40] P. Winsemius, F. Van Kampen, H. Lengkeek, C. Van Went, J. Phys. F Met. Phys. 6 (1976) 1583.
[41] H. Ichimura, I. Ando, Surf. Coating. Technol. 145 (2001) 88–93.
[42] P. Panda, R. Ramaseshan, Ceram. Int. 45 (2019) 1755–1760.
[43] P. Panda, N.G. Krishna, P. Rajput, R. Ramaseshan, Physical Chemistry Chemical Physics, 20, 2018, pp. 29817–29825.